



**HAL**  
open science

## Preferred metabolic pathway of bovine muscle fibre revealed by synchrotron–deep ultraviolet fluorescence imaging

Thierry Astruc, Olivier Loison, Frédéric Jamme, Matthieu M. Refregiers, Annie Venien

### ► To cite this version:

Thierry Astruc, Olivier Loison, Frédéric Jamme, Matthieu M. Refregiers, Annie Venien. Preferred metabolic pathway of bovine muscle fibre revealed by synchrotron–deep ultraviolet fluorescence imaging. *Journal of Spectral Imaging*, 2019, 8, pp.a14. 10.1255/jsi.2019.a14. hal-02431397

**HAL Id: hal-02431397**

**<https://hal.science/hal-02431397>**

Submitted on 7 Jan 2020

**HAL** is a multi-disciplinary open access archive for the deposit and dissemination of scientific research documents, whether they are published or not. The documents may come from teaching and research institutions in France or abroad, or from public or private research centers.

L'archive ouverte pluridisciplinaire **HAL**, est destinée au dépôt et à la diffusion de documents scientifiques de niveau recherche, publiés ou non, émanant des établissements d'enseignement et de recherche français ou étrangers, des laboratoires publics ou privés.

Peer Reviewed Paper **openaccess** [Special Issue on Spectral Imaging in Synchrotron Light Facilities](#)

# Preferred metabolic pathway of bovine muscle fibre revealed by synchrotron–deep ultraviolet fluorescence imaging

Thierry Astruc,<sup>a,\*</sup> Olivier Loison,<sup>b</sup> Frédéric Jamme,<sup>c</sup> Matthieu Réfrégiers<sup>d</sup> and Annie Vénien<sup>e</sup>

<sup>a</sup>UR370 Qualité des Produits Animaux, INRA, 63122 Saint-Genès-Champanelle, France. E-mail: [thierry.astruc@inra.fr](mailto:thierry.astruc@inra.fr),

<https://orcid.org/0000-0001-9528-5827>

<sup>b</sup>UR370 Qualité des Produits Animaux, INRA, 63122 Saint-Genès-Champanelle, France. <https://orcid.org/0000-0001-8167-7977>

<sup>c</sup>Synchrotron SOLEIL, BP48, L'Orme des Merisiers, 91120 Gif-sur-Yvette, France. <https://orcid.org/0000-0002-7398-7868>

<sup>d</sup>Synchrotron SOLEIL, BP48, L'Orme des Merisiers, 91120 Gif-sur-Yvette, France. <https://orcid.org/0000-0002-3281-2308>

<sup>e</sup>UR370 Qualité des Produits Animaux, INRA, 63122 Saint-Genès-Champanelle, France. <https://orcid.org/0000-0002-9270-2151>

The different bovine muscle fibre types I, IIA and IIX are characterised by their preferred metabolic pathway, either oxidative (I, IIA) or glycolytic (IIX), and their contraction speed, either slow-twitch (I) or fast-twitch (IIA, IIX). These physiological specificities are associated with variations in intracellular composition and their fluorescence spectra signatures. We hypothesised that these slight differences in autofluorescence responses could be used to discriminate the muscle fibre types by fluorescence imaging. Serial histological cross-sections of beef longissimus dorsi were performed: the start set was used to identify the metabolic and contractile type of muscle fibres by both immunohistochemistry and immunofluorescence, and the following set was used to acquire synchrotron–deep ultraviolet (UV) autofluorescence images after excitation in the UV range (275 nm and 315 nm). This strategy made it possible to explore the label-free autofluorescence of muscle cells previously subtyped by histochemistry. Glycolytic cells (IIX) showed more intense fluorescence than oxidative cells (I and IIA) with near-90% accuracy. This discrimination is more specifically assigned to the fluorescence of nicotinamide adenine dinucleotide. UV autofluorescence was unable to discriminate contractile type.

**Keywords:** skeletal muscle, fibre type, myosin isoform, UV microspectroscopy, histology, synchrotron radiation

## Introduction

Muscle is composed of elongated muscle cells that measure 10–100 µm in diameter but up to several centimetres in length.<sup>1</sup> They are usually called muscle fibres. These muscle fibres are wrapped in endomysium, a sheath of connective tissue composed of 90% collagen

with the remaining 10% composed of other fibrous proteins, glycoproteins and proteoglycans.<sup>2</sup> Muscle fibres are characterised by their metabolic type (oxidative or glycolytic) and contraction rate (slow or fast-twitch).<sup>3</sup> There are three to four muscle fibre types depending

### Correspondence

T. Astruc ([thierry.astruc@inra.fr](mailto:thierry.astruc@inra.fr))

**Received:** 29 March 2019

**Revised:** 3 June 2019

**Accepted:** 2 July 2019

**Publication:** 18 July 2019

**doi:** 10.1255/jsi.2019.a14

**ISSN:** 2040-4565

### Citation

T. Astruc, O. Loison, F. Jamme, M. Réfrégiers and A. Vénien, "Preferred metabolic pathway of bovine muscle fibre revealed by synchrotron–deep ultraviolet fluorescence imaging", *J. Spectral Imaging* 8, a14 (2019). <https://doi.org/10.1255/jsi.2019.a14>

© 2019 The Authors

This licence permits you to use, share, copy and redistribute the paper in any medium or any format provided that a full citation to the original paper in this journal is given.



on species. The most common nomenclature<sup>4</sup> classifies fibres as types I, IIA, IIB and IIX. Type-I (or slow-twitch oxidative) fibres are characterised by slow-speed contraction and oxidative metabolism, IIA (or fast-twitch oxidative) fibres are characterised by fast contraction and oxidative metabolism, and type-IIX and IIB fibres (or fast-glycolytic) are characterised by fast contraction and glycolytic metabolism. The pure muscle fibres I, IIA, IIX and IIB are also characterised by the fact that they contain the myosin heavy chain isoforms I, Ila, IIX and IIB, respectively, but there are also hybrid fibres containing different isoforms of myosin.<sup>4,5</sup> The proportion of each fibre type is dependent on species, muscle function, age and physical activity. In general, the respiratory muscles and posture muscles are mainly composed of oxidative-metabolism fibres (I and IIA) that are resistant to fatigue. The limb muscles, which can provide violent but short-lived bursts of effort, are often rich in IIB and IIX fibres.

Histochemistry can identify fibre types by highlighting the ATPase activity of pre-incubated fibres in an acid or base bath, and immunohistofluorescence can very robustly identify fibre types using myosin heavy chain isoform-specific, monoclonal antibodies that have been available since the 1990s.<sup>6</sup> However, these identification methods are still time-consuming and expensive to implement, and require specific consumables and equipment.

Protein composition is adapted to physiological function, and thus to fibre type. Type-I and IIA muscle fibres have a higher content of oxidative phosphorylation enzymes<sup>7,8</sup> and respiratory chain cofactors than glycolytic fibres,<sup>9,10</sup> whereas IIX and IIB fibres have higher levels of glycolysis-chain enzymes.<sup>7,8</sup> Different fibre types show very different gene expression patterns,<sup>8,11,12</sup> which points to numerous fibre-type-dependent differences in protein composition. We have previously shown that type-dependent differences in muscle fibre intracellular composition change the optical properties of endogenous fluorophores naturally contained in biological cells.<sup>13,14</sup> Rat muscle fibres excited at 275 nm highlighted a relationship between muscle fibre autofluorescence signal and their sub-type. A 275 nm excitation is likely to induce the autofluorescence of tryptophan ( $\lambda_{\text{exc}}$  277 nm /  $\lambda_{\text{em}}$  360 nm), tyrosine ( $\lambda_{\text{exc}}$  274 nm /  $\lambda_{\text{em}}$  306 nm) and collagen ( $\lambda_{\text{exc}}$  286 nm /  $\lambda_{\text{em}}$  405 nm)<sup>15</sup> while 315 nm partially excites elastin ( $\lambda_{\text{exc}}$  325 nm /  $\lambda_{\text{em}}$  410 nm) and pyridoxine ( $\lambda_{\text{exc}}$  322 nm /  $\lambda_{\text{em}}$  393 nm).<sup>15</sup> Nicotinamide adenine dinucleotide (NADH), which is expected to be

highest in oxidative muscle fibres, presents two maximum excitation peaks—one at  $\lambda_{\text{exc}}$  260 nm and the second at  $\lambda_{\text{exc}}$  345 nm—but the molecule undergoes a partial excitation at both 275 nm and at 315 nm and its emission fluorescence maximum is at 460 nm.<sup>15</sup>

Unfortunately, spectral analysis-based fluorescence microspectroscopy requires time-intensive acquisitions of a huge number of spectra, and any further data pre-processing and statistical analysis steps add more time and require significant expertise. Conversely, ultraviolet (UV) fluorescence imaging, which is also available on the SOLEIL synchrotron's DISCO beamline, takes just seconds to acquire fluorescence images. Here we set out to identify the metabolic and/or contractile types of muscle fibres using UV fluorescence imaging by targeting excitation and emission wavelengths.

## Materials and methods

Figure 1 summarises the experimental design of the study.

### Animals and samples

Two prim'Holstein cows aged seven and eight years were slaughtered at the INRA–Theix experimental slaughterhouse (Theix centre, France). Less than one hour post-mortem, a 10 g piece of longissimus dorsi muscle was extracted from each carcass and taken to the neighbouring laboratory.

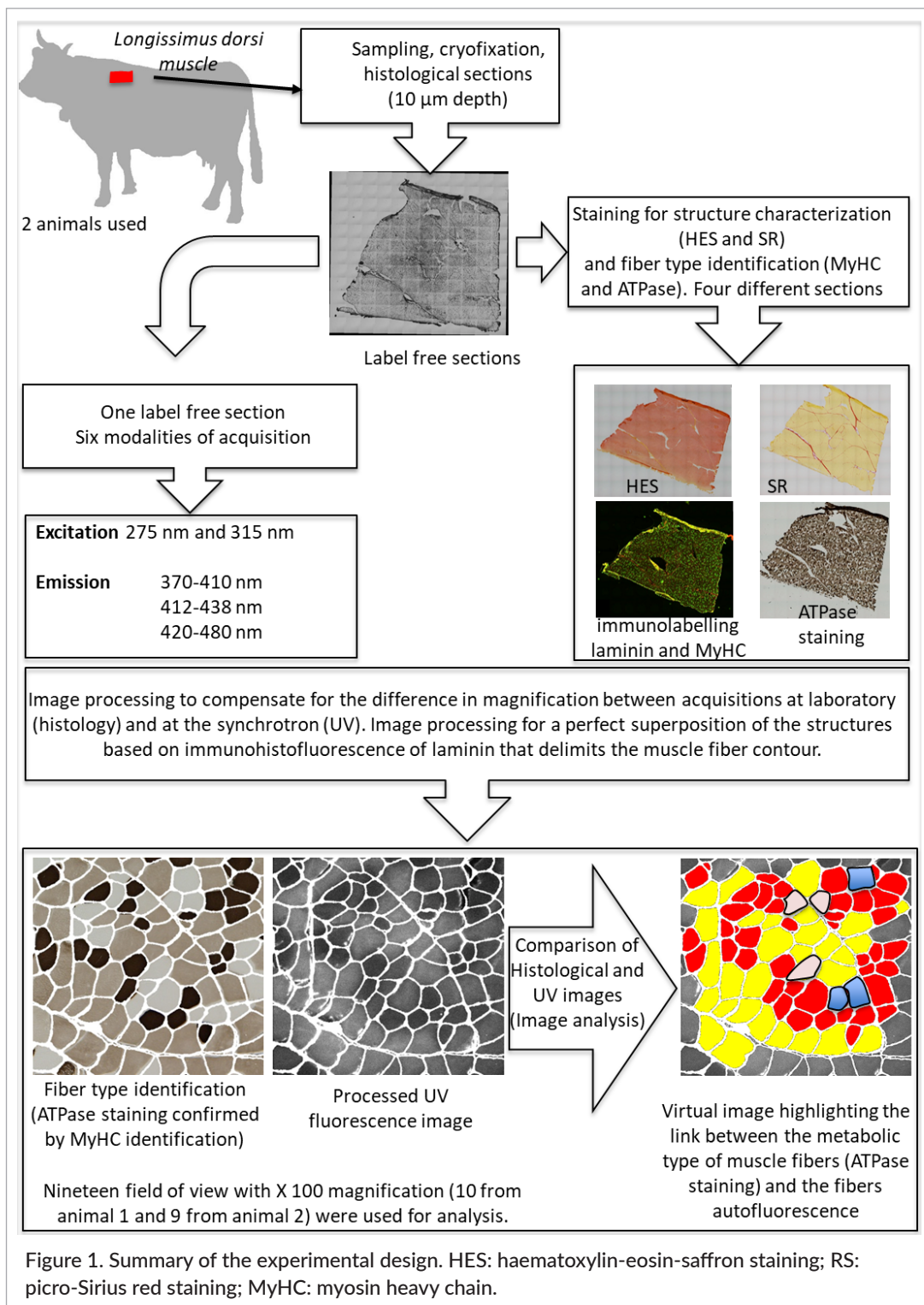
### Sample preparation

Each piece of muscle was used to cut three parallelepipeds of about 1 × 1 × 1.5 cm, with the fibres aligned along the length.

The muscle cubes were positioned on a cork plate with embedding medium (Tissue-Tek) and cryofixed by immersion at  $-160^{\circ}\text{C}$  in liquid nitrogen-cooled ( $-196^{\circ}\text{C}$ ) isopentane. Serial cross-sections (10  $\mu\text{m}$  thick) were cut using a cryostat (Microm, HM 560) then set on glass slides for histological stains and on quartz coverslips for deep ultraviolet (DUV) fluorescence imaging. Sections were stored at  $-20^{\circ}\text{C}$  under vacuum until use.

### Morphological characterisation by histological staining

Sections were stained with haematoxylin-eosin-saffron (HES) to reveal general structure, and picro-



Sirius red (RS) to reveal perimysial and endomysial collagen. After staining, the slides were mounted with synthetic resin (Eukitt, Kindler GmbH & Co, Freiburg, Germany) in order to protect the section over time.

### Muscle fibre-type identification by histochemistry

ATPase staining

ATPase activity was highlighted on histological sections pre-incubated in pH 4.45 solution.<sup>3</sup> Type-I fibres appear

in black, type-IIA in light grey, and types IIB and IIX in dark grey.

#### MyHC isoform identification by immunohistofluorescence

The myosin heavy chain isoforms (MyHC) characterising each muscle fibre type were revealed by immunohistofluorescence.<sup>16</sup>

Fibre types were identified by highlighting the different MyHC isoforms using specific mouse monoclonal antibodies BA-D5 (Deutsche Sammlung von Mikroorganismen und Zellkulturen, Braunschweig, Germany) and S58H2 (AGRO-BIO, La Ferté-St-Aubin, France). BA-D5 revealed MyHC-I (type-I fibres) and S58H2 simultaneously revealed MyHC-I and in a lesser extent MyHC-IIx (type-I and type-IIX fibres). The different primary MyHC antibodies were visualised by an Alexa Fluor 488-labelled goat anti-mouse IgG secondary antibody (A 11001, Invitrogen). In addition, the extracellular matrix protein laminin surrounding the muscle fibre was stained using an anti-laminin primary polyclonal antibody (L9393 Sigma-Aldrich, Saint-Louis, USA) and a cyanine Cy3-labelled secondary antibody (111-165-008, Jackson ImmunoResearch, Cambridge, UK). The S58H2 antibody revealed type-I muscle fibres with a strong fluorescence intensity and type-IIX muscle fibres with a low fluorescence intensity while IIA fibres did not fluoresce. Type-I muscle fibre identification was confirmed by BA-D5 antibody that highlighted only type-I fibres. Controls were performed with no primary antibody to validate the results.

#### Image acquisition

Observations and mosaic image acquisition of the entire sections were performed using a light microscope (Olympus BX 61) coupled to a digital camera (Olympus DP 71) and cellSens Olympus software. ATPase-stained sections were observed in bright-field mode. Immunohistochemistry images were acquired in fluorescence mode (Alexa Fluor 488: 495/519 nm, Cyanine 3: 550/570 nm). Images were acquired at 100× magnification, individual fields of view (FoV) were stitched into a mosaic image, composed of 70–110 images. Each FoV being 1360×1024 pixels and 5.3 MB; the resulting size of the mosaic image was between 9311×8670 pixels and 308 MB, and 13575×9291 pixels and 481 MB for 24 bit.

#### Synchrotron-DUV fluorescence imaging

Synchrotron-DUV imaging was performed on the DISCO beamline of the SOLEIL synchrotron radiation facility (Saint-Aubin, France).<sup>17</sup> Label-free sections were observed through full-field luminescence microscopy (TELEMOS end-station) using an Axio Observer Z1 microscope (Carl Zeiss) with a ×40 Ultrafluar objective. The excitation wavelength was set at 275 nm and reflected toward the sample with a DM-325 dichroic mirror. Fluorescence emission was collected using three filters (bandpass at 370–410 nm, 412–438 nm and 420–480 nm) (Semrock, New York, USA). Acquisition time was set at 30 s for all channels, and 2D fluorescence images were acquired to create a mosaic of images of the whole section for each animal. The mosaic digital images were too large for processing as full captures and so we used the individual FoV that were stitched to form each mosaic image. The mosaic image of animal 1 was composed of 144 FoV and the mosaic image of animal 2 was composed of 80 FoV. Images from the edge of the section and from torn areas were not analysed. Ten FoV images (animal 1) and nine FoV images (animal 2) extracted from mosaic images for each modality were used for analysis.

#### Image analysis

Each FoV image was processed using Fiji software<sup>18</sup> to improve the contrast and localise areas with the highest fluorescent signals. As we did not process the whole mosaic images, but individual images that make them up, the size of the data (1360×1024 pixels and 5.3 MB for each image) was compatible with fast processing using the Fiji software.

Because different microscopes were used to acquire histological images at the laboratory and multimodal fluorescence images on the synchrotron beamline, superimposition of the images required resizing steps. The use of serial sections that are deformed during the sectioning required linear and non-linear transformation to make it possible to overlay histochemistry images with synchrotron-acquired images, which was done using Fiji's TrakEM2 plugin.<sup>19</sup>

Taking the label-free visible field of view as reference, we selected an area encompassing this field of view from the mosaic of the ATPase and immunohistofluorescence stained sections. Using the Fiji's TrakEM2 plugin we first apply an affine transform to rotate, translate and resize the stained image; these transformations resulted in a global overlay of the images. To refine the

overlay, local transformations were obtained by using the Transform Non-linear option of the Fiji's TrakEM2 plugin using 10 to 15 matching points spread all over the reference image and accurately detectable on the image to transform.

### Statistical analysis

To assess the robustness of label-free autofluorescence fibre-type identification compared to histochemical determination, we calculated classification accuracy (CA), recall, specificity and positive predictive value, as follows:

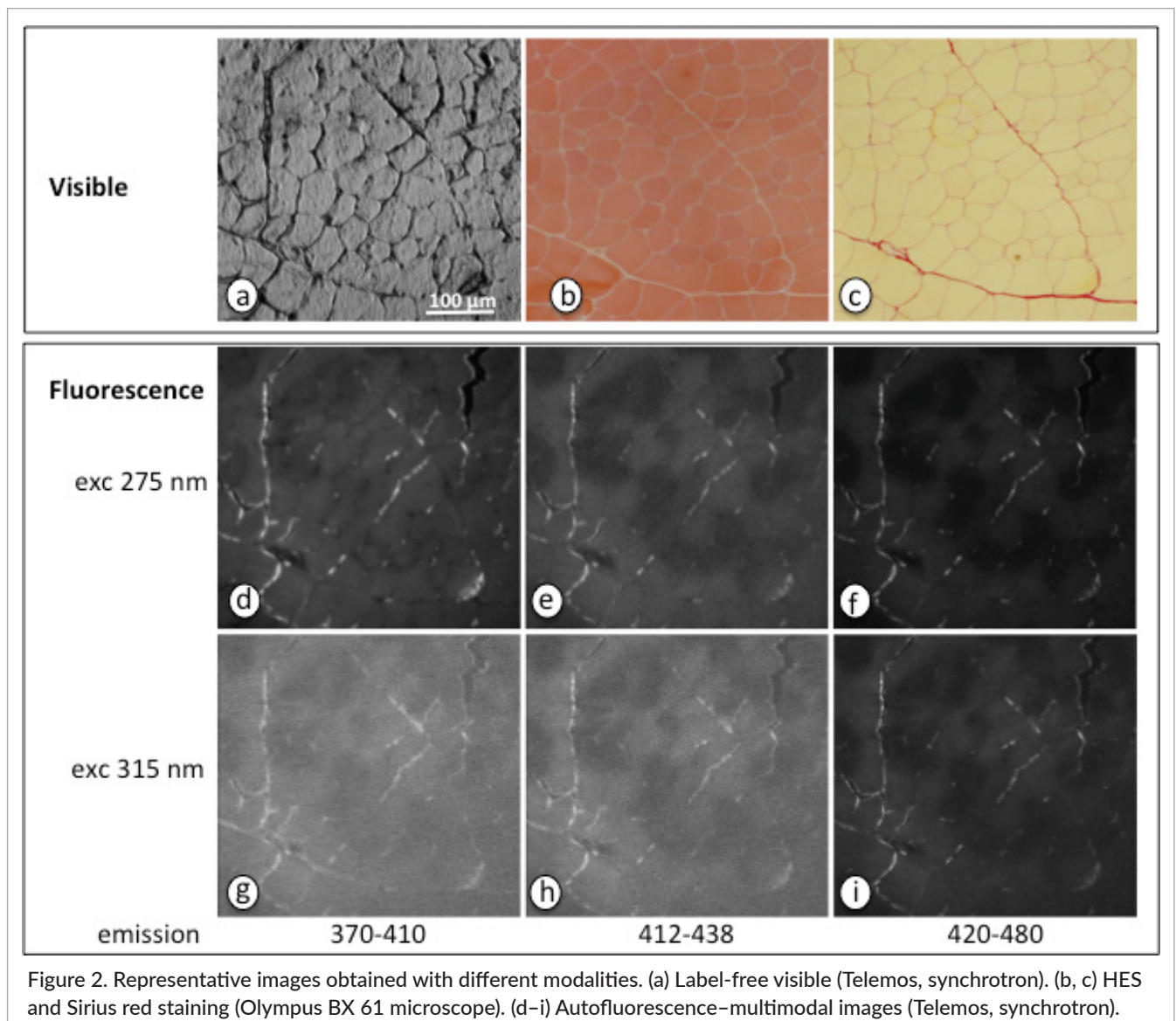
$$\begin{aligned} \text{CA} &= \text{TP} + \text{TN} / \text{TP} + \text{FP} + \text{TN} + \text{FN} \\ \text{Recall} &= \text{TP} / \text{TP} + \text{FN} \\ \text{Specificity} &= \text{TN} / \text{TN} + \text{FP} \\ \text{PPV} &= \text{TP} / \text{TP} + \text{FP} \end{aligned}$$

where TP is true positive, TN is true negative, FN is false negative and FP is false positive.

## Results and discussion

### Characteristics of UV autofluorescence images

A series of representative images is presented in Figure 2. The visible images (a) and DUV fluorescence images (d-i) were rigorously acquired on the same optical field of the same label-free section by modifying the modes of excitation and emission of fluorescence. Histological staining with HES and Sirius red was performed on serial sections. The visible image of the unstained section (a) distinguishes



the muscle cells, which is confirmed by comparison with images from histological staining (b and c). In black-and-white spectral images, degree of fluorescence is reflected by the higher or lower greyscale level: fluorescent zones are clear whereas low-fluorescent zones are dark.

#### Connective tissue fluorescence

The DUV fluorescence images (Figure 2, d-i) reveal fluorescent white lines that correspond to the arrays of connective tissue that make up the perimysium, perfectly identifiable after histological staining (Figure 2b and c). These white fillets are due to autofluorescence of collagen ( $\lambda_{exc}$  286 nm/ $\lambda_{em}$  405 nm) and to a lesser extent elastin ( $\lambda_{exc}$  325 nm/ $\lambda_{em}$  410 nm) that are co-located in the extracellular matrix.<sup>20,21</sup> The excitation and fluorescence emission peaks of these compounds are widely spread<sup>15</sup> and both the collagen and elastin components are co-excited,<sup>22</sup> which explains why their fluorescence is more or less visible regardless of the emission filters used. Collagen, the predominant compound of the endomysium that envelops each muscle fibre, is perfectly visible after Sirius red staining (Figure 2c) but its autofluorescence is insufficient to visualise the contour of the cells using the exc/em bandpass 275/370–410 nm (Figure 2d). The endomysium has been shown to contain both type-I and type-III collagen as major components<sup>23</sup> that emit fluorescence.<sup>24</sup> The near absence of endomysium fluorescence is probably related to the preparation of the sections and their time in storage before use on the synchrotron's DISCO beamline. Indeed, Swatland<sup>24</sup> observed a fading of the 420 nm fluorescence peak of reticular collagen perimysial fibres after prolonged drying of frozen sections, storage of mounted sections and brief exposure to UV light.

#### Muscle fibre fluorescence

The slightly better resolution of muscle fibres in Figure 2d is perfectly consistent with the results of Skjervold *et al.*,<sup>25</sup> who observed a peak of fluorescence emission at 330 nm in muscle fibres after excitation at 290 nm. This fluorescence emission is mainly due to the autofluorescence of tryptophan.<sup>22,26,27</sup> The contrast variations observed on the fluorescence images do not seem specific to tryptophan because they are observed on the other images, particularly with the bandpass at 412–438 nm and 420–480 nm. The best contrast is observed for Figure 2f at 275/420–480 nm which suggests that some muscle fibres are more fluorescent than others.

The other fluorophores most likely to be involved in the autofluorescence of UV-excited muscle fibres are NADH (260 and 345/400–600 nm)<sup>15,27–29</sup> and pyridoxine (252 and 322/400–550 nm).<sup>15</sup> Their excitation is lower at 275 nm. Illumination at 275 nm and at 315 nm results in the same excitation of NADH whereas pyridoxine is substantially more excited at 315 nm.<sup>15</sup> The autofluorescence of tyrosine (274/306 nm) cannot be observed under our conditions because there is no filter able to visualise its fluorescence emission.<sup>15,27</sup>

#### Fibre-type identification

The typing results show that bovine longissimus dorsi is composed of 26% type-I fibres, 28% type-IIA fibres and 46% type-IIIX fibres ( $n = 1416$  muscle fibres). These values are close to the 30% I, 20% IIA and 50% IIX observed in bovine longissimus dorsi muscle by Chriki *et al.*<sup>30</sup> and Johnston *et al.*<sup>31</sup> The distribution of the different fibre types is homogeneous, as shown in Figure 3.

An increase in magnification shows that immunostaining using Ac S58H2 (Figure 4) allows all three fibre types to

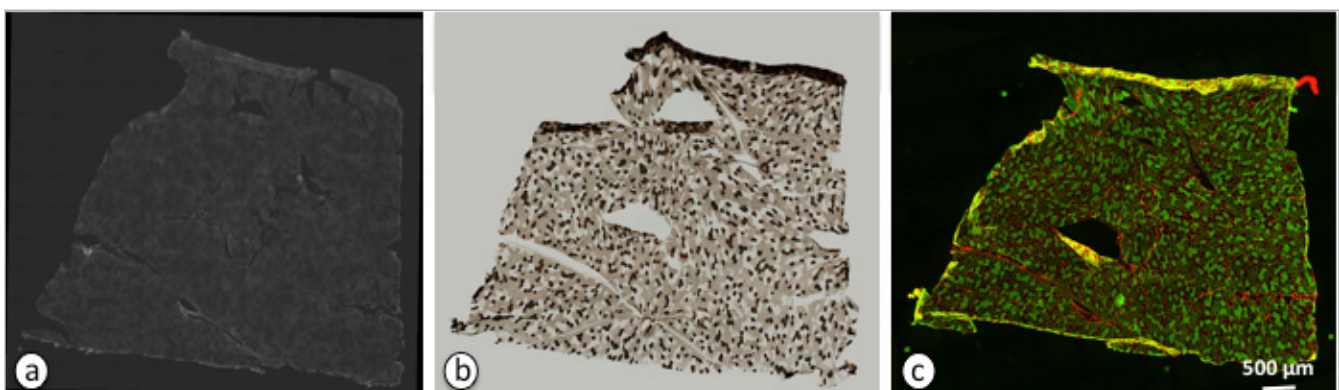


Figure 3. Mosaic of individual digital images of three serial sections. (a) Label-free 275/420–480 nm autofluorescence, (b) ATPase staining, (c) MyHC-I and IIX (S58H2) and laminin double-immunolabelling.

be identified: the labelling is very intense for type-I fibres, less intense for type-IIIX fibres and type-IIA fibres are not marked. This result fits perfectly with fibre-type identification by ATPase staining.

### Relationship between variations of autofluorescence and fibre type

As the best autofluorescence contrast was found for the 275/420–480nm tandem, only images from this acquisition mode were used in data processing and analysis. Visual comparison of the 275/420–480nm autofluorescence image with the visible image (Figure 4) suggests that some muscle fibres are less contrasted (thus more fluorescent) than others.

To check whether these differences in contrast are associated with fibre type, it is necessary to be able to superimpose the autofluorescence images with the histological typing images. However, the label-free images (visible and UV fluorescence) were acquired at the synchrotron with the same microscope and rigor-

ously on the same optical field with only the acquisition modalities modified, while the histological images used for fibre-type identification were acquired in the laboratory on serial sections and with a different microscope than that available at the synchrotron. The magnifications were, therefore, not identical, and the sections were oriented differently on their slides. In addition, cutting histological sections causes deformations that do not allow a perfect superimposition of the serial sections and thus of cells and tissue components without prior image processing. The extracellular matrix network, identified by laminin labelling, was used to highlight the cell contour on label-free UV fluorescence images using Fiji's TrakEM2 plugin (Figure 5).

Observation of the image resulting from superposition of the laminin matrix over the label-free UV fluorescence image indicates that the variations in fluorescence intensity of the muscle fibres are related to the metabolic type of the cells. Indeed, the glycolytic type-IIIX fibres have

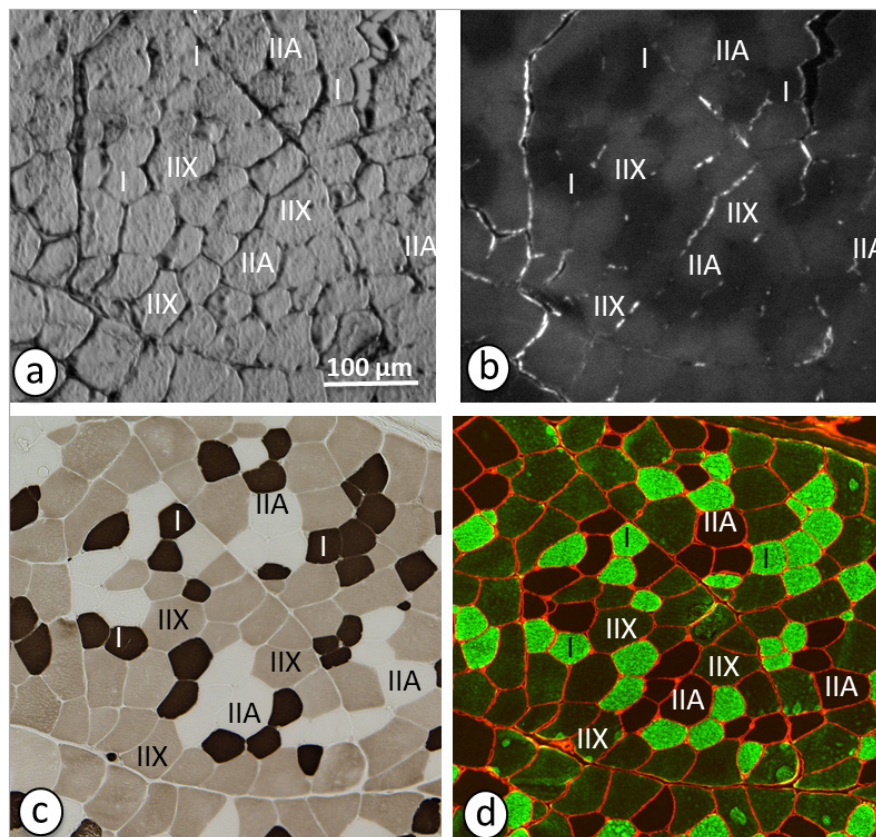


Figure 4. Comparison of fluorescence image and typing images of the same area. (a) Label-free visible image, (b) label-free fluorescence image (275/420–480nm), (c) ATPase staining, (d) immunohistofluorescence of MyHC with 58H2 monoclonal antibody and anti-laminin antibody.



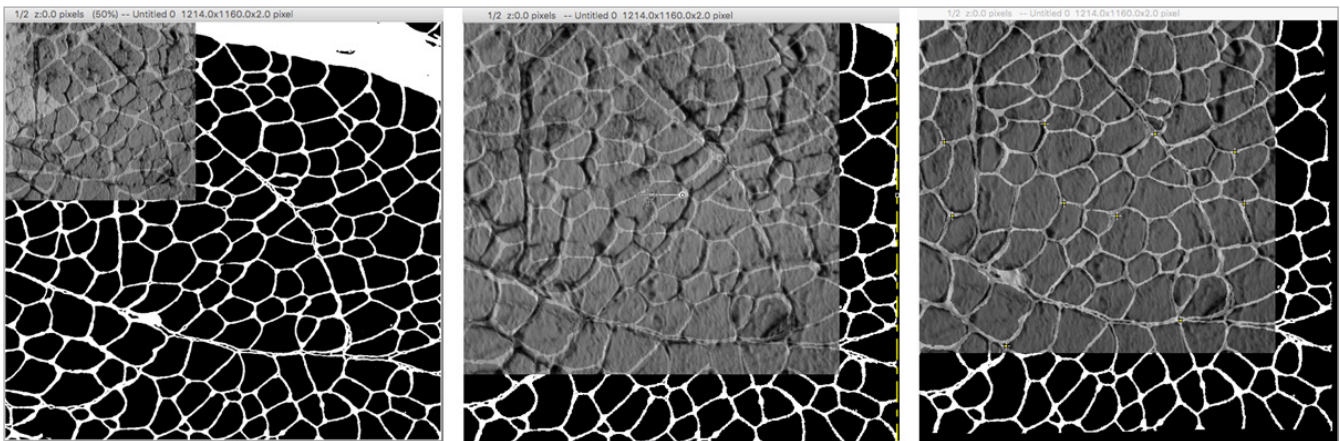


Figure 5. Image processing to overlay histochemical images on synchrotron images. (a) Visible image as reference and laminin network to be modified, (b) overlay of the laminin network after linear transformation, (c) final overlay after linear and non-linear transformation.

higher fluorescence intensity than the oxidative type-I and IIA fibres (Figures 4 and 6).

For the purpose of automated determination, the fibres were sorted on their average greyscale level. A visual representation of the characterisation is given in Figure 6. The metabolic type is identified with almost 90% success (Table 1).

Type-I fibres are predicted with high precision (370 out of 375 fibres were well identified; Recall=0.99) whereas the prediction is much less accurate for type-IIA fibres (310 out of 392 fibres well identified; Recall=0.79) and type-IIX fibres (575 out of 649 fibres well identified; Recall=0.88). The type-IIA fibres poorly identified in multimodal fluorescence imaging are therefore generally type-IIX, and vice versa. Type-I fibres are slow-twitch and

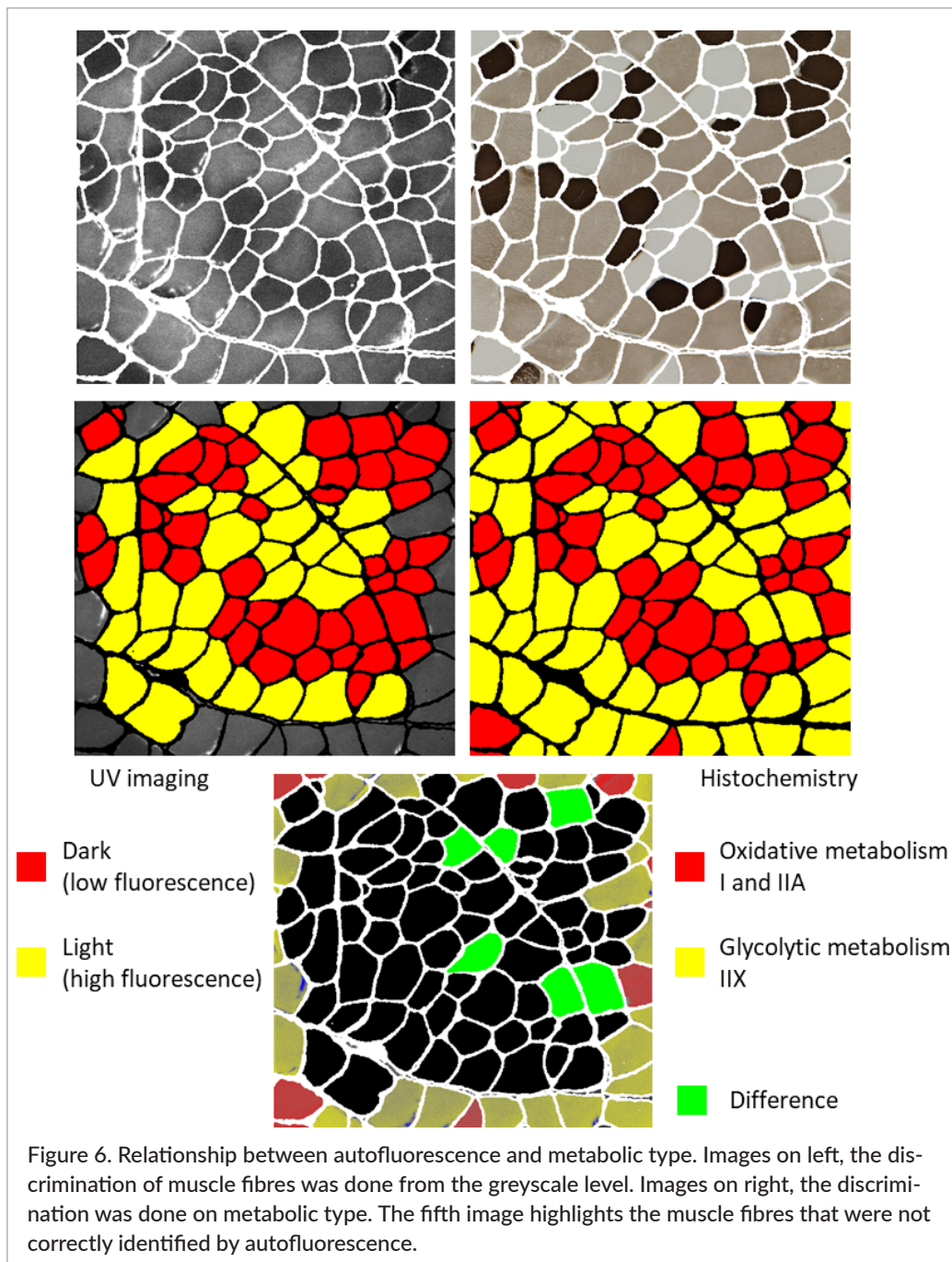
their metabolism is the most oxidative in most species, including cattle. These type-I fibres have a very different composition to type-IIA fibres and especially to type-IIX fibres, which explains their excellent identification by autofluorescence. Type-IIA fibres are fast-twitch, like type-IIX, but their metabolism is intermediate between type-I and type-IIX fibres. Type-IIX fibres are the most glycolytic in cattle that do not contain type-IIB fibre (except for some breeds that can contain tiny amounts of type-IIB fibres), but they are also capable, in small proportions, of oxidative metabolism. The characteristics and, therefore, intracellular composition of the type-IIA fibres are, therefore, closer to type-IIX fibres than to type-I fibres, which may explain the lesser precision in the metabolic type discrimination of the type-II fibres.

**Table 1. Robustness of the metabolic type prediction ( $n = 1416$  muscle fibres).**

Classification accuracy	0.89
Recall	0.89
Specificity	0.89
Positive predictive value	0.87

**Table 2. Accuracy of prediction.**

	Number (identified by histology)	Well identified	Badly identified
Oxidative type-I	375	370	5
Oxidative type-IIA	392	310	82
Glycolytic type-IIX	649	575	74



Identifying the fluorophore(s) involved is a difficult challenge. The results indicate that type-IIX fibres have higher fluorescence intensity after excitation at 275 nm. This fluorescence is, therefore, linked to glycolytic type. The intracellular fluorophores capable of responding are NADH and pyridoxine which emit fluorescence between 420 nm and 480 nm.

Pyridoxine activates glycogen phosphorylase, which is involved in muscle glycogenolysis.<sup>32-35</sup> However, glycogenolysis is the initial step in the energy metab-

olism of all muscle fibres, regardless of fibre type. Glycogen phosphorylase, which catalyses glycogen degradation, is at least 1.5 times more active in glycolytic-metabolism fibres (IIB–IIX) than in oxidative-metabolism fibres which need a lot of immediately available energy.<sup>36</sup> However, the low fluorescence intensity of images acquired in the 315/370–410 nm modality suggests that pyridoxine ( $\lambda_{exc}$  322 nm /  $\lambda_{em}$  393 nm) is only weakly involved in the autofluorescence response.

The other sarcoplasmic compound capable of autofluorescence in our experimental conditions is NADH. Its maximum emission is at 460nm when it is excited in the UV region.<sup>15</sup> *In vivo*, this compound is mainly involved in the cellular respiration that occurs in the mitochondria of cells with oxidative metabolism (type-I and IIA fibres).<sup>9</sup> Our protocol performed muscle sampling in an experimental slaughterhouse, about one hour after slaughter. However, as soon as the animal dies, the muscle fibres maintain their homeostasis exclusively by glycolytic metabolism, which is anaerobic. Adenosine triphosphate (ATP) is then essentially regenerated by glycogenolysis, followed by glycolysis and lactic fermentation.<sup>37</sup> In the reaction chain of glycolysis, glyceraldehyde 3-phosphate is dehydrogenated to 1,3-diphosphoglycerate by the reduction of NAD to NADH which is re-oxidised to NAD<sup>+</sup> during the conversion of pyruvate to lactate.<sup>37,38</sup> Glycolytic fibres, which even *in vivo* essentially use this metabolic pathway, perform better than oxidative fibres to rapidly produce ATP anaerobically.<sup>4,37</sup> As long as there is glycogen in the cells, the rapid metabolism of type-IIX fibres is likely to induce a higher cytoplasmic NADH content than in the oxidative fibres (I and IIA), in agreement with our results.

## Conclusion

The different types of muscle fibres are characterised by their speed of contraction (slow or fast) and their preferential metabolic pathway (oxidative or glycolytic). These characteristics result in type-dependent variations in the intracellular composition of the fibres.<sup>8</sup> In our experimental conditions, autofluorescence was unable to discriminate the fibres on their speed of contraction. However, despite their low fluorescence intensity, the oxidative-metabolism fibres were very accurately distinguishable from glycolytic-metabolism fibres. Glycolytic-metabolism fibres generate a slightly more intense autofluorescence. Type-I fibres showed the lowest fluorescence and were almost always correctly classified as oxidative from autofluorescence images. The CA was lower for type-IIA as oxidative and type-IIX as glycolytic, probably due to their physiological proximity. The fluorescence emitted by glycolytic fibres is assigned to sarcoplasmic NADH.

Incomplete fluorescence of the endomysium collagen (which surrounds the muscle fibres) proved a major bottleneck for image processing, and forced us to rely

on immunolabelling laminin to accurately delineate the cell contour. The next challenges are to better highlight the autofluorescence of collagen, and to gain a better contrast of autofluorescence images by improving image acquisition and pretreatment protocols.

## References

1. A. Listrat, B. Leuret, I. Louveau, T. Astruc, M. Bonnet, L. Lefaucheur, B. Picard and J. Bugeon, "How muscle structure and composition influence meat and flesh quality", *Scientific World Journal* **2016**, 3182746 (2016). <https://doi.org/10.1155/2016/3182746>
2. A.R. Gillies and R.L. Lieber, "Structure and function of the skeletal muscle extracellular matrix", *Muscle Nerve* **44(3)**, 318 (2011). <https://doi.org/10.1002/mus.22094>
3. M.H. Brooke and K.K. Kaiser, "Three 'myosin adenosine triphosphatase' systems: the nature of their pH lability and sulfhydryl dependence", *J. Histochem. Cytochem.* **18(9)**, 670 (1970). <https://doi.org/10.1177/18.9.670>
4. S. Schiaffino and C. Reggiani, "Fiber types in mammalian skeletal muscles", *Physiol. Rev.* **91(4)**, 1447 (2011). <https://doi.org/10.1152/physrev.00031.2010>
5. D. Pette and R.S. Staron, "Myosin isoforms, muscle fiber types, and transitions", *Microsc. Res. Tech.* **50(6)**, 500 (2000). [https://doi.org/10.1002/1097-0029\(20000915\)50:6<500::AID-JEMT7>3.0.CO;2-7](https://doi.org/10.1002/1097-0029(20000915)50:6<500::AID-JEMT7>3.0.CO;2-7)
6. T. Astruc and A. Vénien, "Muscle fibre types and beef quality", in *Ensuring Safety and Quality in the Production of Beef*, Ed by M. E. Dikeman. Burleigh Dodds Science Publishing, Cambridge, UK (2017).
7. L. Lefaucheur, "A second look into fibre typing—relation to meat quality", *Meat Sci.* **84(2)**, 257 (2010). <https://doi.org/10.1016/j.meatsci.2009.05.004>
8. F. Chemello, C. Bean, P. Cancellara, P. Laveder, C. Reggiani and G. Lanfranchi, "Microgenomic analysis in skeletal muscle: expression signatures of individual fast and slow myofibers", *PLoS One* **6(2)**, e16807 (2011). <https://doi.org/10.1371/journal.pone.0016807>
9. A. Mayevsky and G.G. Rogatsky, "Mitochondrial function *in vivo* evaluated by NADH fluorescence: from animal models to human studies", *Am. J.*

- Physiol. Cell Physiol.* **292**(2), C615 (2007). <https://doi.org/10.1152/ajpcell.00249.2006>
10. J.M. Ren, J. Henriksson, A. Katz and K. Sahlin, "NADH content in type I and type II human muscle fibres after dynamic exercise", *Biochem. J.* **251**(1), 183 (1988). <https://doi.org/10.1042/bj2510183>
  11. Y.M. Choi and B.C. Kim, "Muscle fiber characteristics, myofibrillar protein isoforms, and meat quality", *Livest. Sci.* **122**(2–3), 105 (2009). <https://doi.org/10.1016/j.livsci.2008.08.015>
  12. Y. Ogura, H. Naito, R. Kakigi, N. Ichinoseki-Sekine, M. Kurosaka and S. Katamoto, "Alpha-actinin-3 levels increase concomitantly with fast fibers in rat soleus muscle", *Biochem. Biophys. Res. Commun.* **372**(4), 584 (2008). <https://doi.org/10.1016/j.bbrc.2008.05.059>
  13. C. Chagnot, A. Vénien, F. Jamme, M. Réfrégiers, M. Desvaux and T. Astruc, "Hyperspectral deep ultraviolet autofluorescence of muscle fibers is affected by postmortem changes", *J. Agric. Food Chem.* **63**(19), 4782 (2015). <https://doi.org/10.1021/acs.jafc.5b00668>
  14. C. Chagnot, A. Vénien, F. Peyrin, F. Jamme, M. Réfrégiers, M. Desvaux and T. Astruc, "Deep UV excited muscle cell autofluorescence varies with the fibre type", *Analyst (Lond.)* **140**(12), 4189 (2015). <https://doi.org/10.1039/C5AN00172B>
  15. F. Jamme, S. Kascakova, S. Villette, F. Allouche, S. Pallu, V. Rouam and M. Réfrégiers, "Deep UV autofluorescence microscopy for cell biology and tissue histology", *Biol. Cell* **105**(7), 277 (2013). <https://doi.org/10.1111/boc.201200075>
  16. B. Meunier, B. Picard, T. Astruc and R. Labas, "Development of image analysis tool for the classification of muscle fibre type using immunohistochemical staining", *Histochem. Cell Biol.* **134**(3), 307 (2010). <https://doi.org/10.1007/s00418-010-0733-7>
  17. A. Giuliani, F. Jamme, V. Rouam, F. Wien, J.-L. Giorgetta, B. Lagarde, O. Chubar, S. Bac, I. Yao, S. Rey, C. Herbeaux, J.-L. Marlats, D. Zerbib, F. Polack and M. Réfrégiers, "DISCO: a low-energy multipurpose beamline at synchrotron SOLEIL", *J. Synchrotron Radiat.* **16**(Pt 6), 835 (2009). <https://doi.org/10.1107/S0909049509034049>
  18. J. Schindelin, I. Arganda-Carreras, E. Frise, V. Kaynig, M. Longair, T. Pietzsch, S. Preibisch, C. Rueden, S. Saalfeld, B. Schmid, J.-Y. Tinevez, D.J. White, V. Hartenstein, K. Eliceiri, P. Tomancak and A. Cardona, "Fiji: an open-source platform for biological-image analysis", *Nat. Methods* **9**(7), 676 (2012). <https://doi.org/10.1038/nmeth.2019>
  19. A. Cardona, S. Saalfeld, J. Schindelin, I. Arganda-Carreras, S. Preibisch, M. Longair, P. Tomancak, V. Hartenstein and R.J. Douglas, "TrakEM2 software for neural circuit reconstruction", *PLoS One* **7**(6), e38011 (2012). <https://doi.org/10.1371/journal.pone.0038011>
  20. A.J. Bailey and N.D. Light, *Connective Tissue in Meat and Meat Products*. Elsevier, London (1989).
  21. T. Astruc, F. Peyrin, A. Vénien, R. Labas, M. Abrantes, P. Dumas and F. Jamme, "In situ thermal denaturation of myofibre sub-type proteins studied by immunohistofluorescence and synchrotron radiation FT-IR microspectroscopy", *Food Chem.* **134**(2), 1044 (2012). <https://doi.org/10.1016/j.foodchem.2012.03.012>
  22. V. Zubkova, F. Jamme, S. Kascakova, F. Chiappini, F. Le Naour and M. Réfrégiers, "Single vs. two-photon microscopy for label free intrinsic tissue studies in the UV light region", *Analyst (Lond.)* **139**(11), 2663 (2014). <https://doi.org/10.1039/C4AN00203B>
  23. N. Light and A.E. Champion, "Characterization of muscle epimysium, perimysium and endomysium collagens", *Biochem. J.* **219**(3), 1017 (1984). <https://doi.org/10.1042/bj2191017>
  24. H.J. Swatland, "Fluorimetry of bovine myotendon junction by fibre-optics and microscopy of intact and sectioned tissues", *Histochem. J.* **19**(5), 276 (1987). <https://doi.org/10.1007/BF01675687>
  25. P.O. Skjervold, R.G. Taylor, J.P. Wold, P. Berge, S. Abouelkaram, J. Culioli and E. Dufour, "Development of intrinsic fluorescent multispectral imagery specific for fat, connective tissue, and myofibers in meat", *J. Food Sci.* **68**(4), 1161 (2003). <https://doi.org/10.1111/j.1365-2621.2003.tb09618.x>
  26. A. Sahar and É. Dufour, "Classification and characterization of beef muscles using front-face fluorescence spectroscopy", *Meat Sci.* **100**, 69 (2015). <https://doi.org/10.1016/j.meatsci.2014.09.142>
  27. Y. Kumamoto, A. Taguchi and S. Kawata, "Deep-ultraviolet biomolecular imaging and analysis", *Adv. Opt. Mater.* **1**, (2018). <https://doi.org/10.1002/adom.201801099>
  28. E. Dufour, J.P. Frenchia and E. Kane, "Development of a rapid method based on front-face fluorescence

- spectroscopy for the monitoring of fish freshness", *Food Res. Int.* **36(5)**, 415 (2003). [https://doi.org/10.1016/S0963-9969\(02\)00174-6](https://doi.org/10.1016/S0963-9969(02)00174-6)
29. A.C. Croce and G. Bottiroli, "Autofluorescence spectroscopy and imaging: a tool for biomedical research and diagnosis", *Eur. J. Histochem.* **58(4)**, 2461 (2014). <https://doi.org/10.4081/ejh.2014.2461>
30. S. Chriki, B. Picard, C. Jurie, M. Reichstadt, D. Micol, J.-P. Brun, L. Journaux and J.-F. Hocquette, "Meta-analysis of the comparison of the metabolic and contractile characteristics of two bovine muscles: longissimus thoracis and semitendinosus", *Meat Sci.* **91(4)**, 423 (2012). <https://doi.org/10.1016/j.meatsci.2012.02.026>
31. D.M. Johnston, W.G. Moody, J.A. Boling and N.W. Bradley, "Influence of breed type, sex, feeding systems, and muscle bundle size on bovine fiber type characteristics", *J. Food Sci.* **46(6)**, 1760 (1981). <https://doi.org/10.1111/j.1365-2621.1981.tb04480.x>
32. D. Palm, H.W. Klein, R. Schinzel, M. Buehner and E.J. Helmreich, "The role of pyridoxal 5'-phosphate in glycogen phosphorylase catalysis", **29(5)**, 1099 (1990). <https://doi.org/10.1021/bi00457a001>
33. S. Sato, T. Ohi, I. Nishino and H. Sugie, "Confirmation of the efficacy of vitamin B6 supplementation for McArdle disease by follow-up muscle biopsy", *Muscle Nerve* **45(3)**, 436 (2012). <https://doi.org/10.1002/mus.22290>
34. R. Izumi, N. Suzuki, K. Kato, H. Warita, M. Tateyama, I. Nakashima and Y. Itoyama, "A case of McArdle disease: efficacy of vitamin B6 on fatigability and impaired glycogenolysis", *Intern. Med.* **49(15)**, 1623 (2010). <https://doi.org/10.2169/internalmedicine.49.3525>
35. R.G. Haller, W.B. Dempsey, H. Feit, J.D. Cook and J.P. Knochel, "Low muscle levels of pyridoxine in McArdle's syndrome", *Am. J. Med.* **74(2)**, 217 (1983). [https://doi.org/10.1016/0002-9343\(83\)90614-9](https://doi.org/10.1016/0002-9343(83)90614-9)
36. J.R. Zierath and J.A. Hawley, "Skeletal muscle fiber type: influence on contractile and metabolic properties", *PLoS Biol.* **2(10)**, e348 (2004). <https://doi.org/10.1371/journal.pbio.0020348>
37. J.R. Bendall, "Post mortem changes in muscle", in *Structure and Function of Muscle*, Ed by G.H. Bourne. Academic Press, New York 243 (1973).
38. H. Westerblad, J.D. Bruton and A. Katz, "Skeletal muscle: energy metabolism, fiber types, fatigue and adaptability", *Exp. Cell Res.* **316(18)**, 3093 (2010). <https://doi.org/10.1016/j.yexcr.2010.05.019>